Article

Received: 03.11.2023
Accepted: 12.12.2023

UDC 538.971 https://doi.org/10.31489/2024PH1/13-22

M.M. Kubenova[1*], K.A. Kuterbekov[1], M.Kh. Balapanov[2], R.Kh. Ishembetov[2], G.D. Kabdrakhimova[1], R.A. Alina[1], M. Tatay[1], R. Ildos[1]

[1]*L.N. Gumilyov Eurasian National University, 2 Satpayev str., 010008 Astana, Kazakhstan;*
[2]*Ufa University of Science and Technology, 32 Zaki Validi str., 450076 Ufa, Bashkortostan, Russia*
[*]*Corresponding author's e-mail: kubenova.m@yandex.kz*

Thermal properties of Cu_2S binary copper sulfides

Copper chalcogenides have a complex electronic structure due to the interaction of hybridized s- and p-states of chalcogen forming a valence band with 3d states of copper, which greatly complicates the interpretation of temperature dependences of kinetic parameters having a nonmonotonic character. Cu_2S copper sulfide is an effective thermoelectric material, so it is interesting to study its kinetic parameters of solid solutions that it forms with alkali metals. The nonstoichiometry of chalcogenides can be easily controlled electrochemically, therefore, the task of selecting the optimal composition according to the cationic sublattice is quite feasible. The paper presents experimental studies of the properties of Cu_2S binary copper sulfide. Copper chalcogenides have a complex electronic structure due to the interaction of hybridized s- and p-states of chalcogen forming a valence band with 3d states of copper, which greatly complicates the interpretation of temperature dependences of kinetic parameters having a nonmonotonic character. For the Cu_2S sample, rather low values of the electron thermal EMF coefficient of the sample from 0.05 mV/K to 0.25 mV/K were found, which are more typical for metals than for semiconductors. The thermal conductivity of the Cu_2S sample is quite low, it rises to 0.3 W/m*K at a phase transition of about 380 K and does not fall below 0.2 W/m*K. Thus, the nonstoichiometry of chalcogenides can be easily controlled electrochemically, therefore, the task of selecting the optimal composition according to the cationic sublattice is quite feasible. In addition, to improve the thermoelectric properties of Cu_2S, it can be achieved by alloying alkali metals into a binary copper sulfide matrix.

Keywords: thermoelectric materials, copper sulfide, crystal structure, conductivity, thermal conductivity, Seebeck coefficient, superionic conductors.

Introduction

Copper sulfide has proven to be a more efficient material in solar cells [1]. CES with Cu_2S–CDs heterojunction attract attention due to the real possibility of their wide application as ground-based photovoltaic energy converters; in addition, the study of the properties of the heterojunction is of considerable scientific interest.

One of the first methods for producing a thin Cu_2S film in a Cu_2S–CDs solar cell consists in dipping a substrate with a deposited CDs layer with a solution heated to 90 °C containing copper ions, in which 2 g of NaCl and 6 g of CuCl per 1 liter of H_2O (pH ~3...4). As a result of the substitution reaction, a Cu_2S film with a thickness of 30 nm is formed on the surface of CDs. The efficiency of such a solar cell reaches 10 % [1].

Copper selenide has also performed well in the composition of solar cells. $Cu_{2-x}Se$-*n*-Si hetero junction elements with an efficiency of 8.8 % were manufactured on monocrystalline *n*-Si substrates by $Cu_{2-x}Se$ thermal sputtering [2, 3]. During spraying, a pre-synthesized material is used, which is evaporated either from the liquid phase or from a red-hot rod. With such a technology for manufacturing solar cells, non-stoichiometric copper selenide can be used, obtained according to the methods developed in this project.

Modern silicon solar cells have achieved very high efficiency — about 25 %. One of the interesting directions is the use of quantum dots, which makes it possible to obtain layers with different band gap widths from the same material, for example, silver sulfide. It is in optical devices that nanotechnology products are used, including in SE.

Experimental part

The technique of synthesis of $Cu_{2-x}S$ nanodiscs. The following chemicals are used for the synthesis of nanodiscs: copper (I) chloride (CuCl, 99.995 %), oleylamine (OAm, 70 %), sulfur (S) powder (99.98 %) and trioctylphosphine oxide (TOPO, technical grade 90 %).

The synthesis of Cu_2S nanoplates is carried out in one stage. The diameter of the resulting discs is about 20–30 nm, the thickness is 3–5 nm.

The required amount of CuCl (0.25–0.5 mmol ― depending on the desired nonstoichiometry *x*) is mixed with 1 mmol of sulfur powder, 4 g of trioctylphosphinoxide (TOPO) and 10 ml of oleylamine (OAm). The solution is degassed at room temperature in a nitrogen atmosphere, then heated to 85 °C and maintained at this temperature for 1 hour. After that, the heating jacket is Cu_2S removed and 20–30 ml of ethanol is injected, the temperature decreases to ~ 40 °C. The resulting Cu_2S powder is collected by centrifugation at 9000 rpm for 1 min. The collected Cu_2S samples are re-dispersed in chloroform. This procedure is repeated twice to clean the prepared Cu_2S. Then the obtained samples are dried at a temperature of 40–50 °C.

An X-ray phase analysis of the obtained compacted nanocrystalline and powder samples was performed at room temperature (Tables 1–3). The identification of X-ray reflexes was carried out.

Table 1

Results of RFA $Cu_{1.85}S$

No.	2 θ, (deg)	d, (ang.)	Height (cps)	FWHM (deg)	Size (ang.)	Phase name	Chemical formula
1	24.705(7)	3.6008(11)	163(26)	0.10(2)	830(172)	Unknown	
2	26.533(11)	3.3567(14)	479(45)	0.121(16)	706(95)	Roxbyite(2,-3,2),chalcocite, high, copper(I) sulfide(1,0,0)	$Cu_{29}S_{16}$, Cu_2S
3	29.783(11)	2.9974(11)	460(44)	0.15(2)	566(93)	Roxbyite(2,-4,0),chalcocite, high, copper(I) sulfide(1,0,1)	$Cu_{29}S_{16}$, Cu_2S
4	31.209(8)	2.8636(8)	763(57)	0.121(10)	714(59)	Roxbyite(1,3,-4)	$Cu_{29}S_{16}$
5	34.059(4)	2.6302(3)	866(60)	0.096(8)	904(76)	Roxbyite(5,1,0)	$Cu_{29}S_{16}$
6	35.392(3)	2.5341(2)	1627(83)	0.071(6)	1233(97)	Roxbyite(0,4,-4)	$Cu_{29}S_{16}$
7	36.377(3)	2.4678(2)	2243(97)	0.122(5)	717(32)	Unknown	
8	37.920(10)	2.3708(6)	940(63)	0.232(10)	378(17)	Roxbyite(3,-2,5),chalcocite, high, copper(I) sulfide(1,0,2)	$Cu_{29}S_{16}$, Cu_2S
9	38.55(5)	2.333(3)	225(31)	0.71(6)	123(11)	Roxbyite(1,-5,-3)	$Cu_{29}S_{16}$
10	42.244(12)	2.1376(6)	460(44)	0.19(3)	478(72)	Unknown	
11	43.296(3)	2.08806(13)	389(40)	0.066(10)	1352(198)	Sulfur-III(1,0,-1)	S
12	46.309(13)	1.9590(5)	294(35)	0.30(7)	304(73)	Roxbyite(6,2,3)	$Cu_{29}S_{16}$
13	46.909(9)	1.9353(4)	1098(68)	0.257(14)	352(19)	Roxbyite(0,6,-4),chalcocite, high, copper(I) sulfide(1,1,0)	$Cu_{29}S_{16}$, Cu_2S
14	47.99(3)	1.8942(13)	147(25)	0.17(7)	522(216)	Roxbyite(5,-5,0)	$Cu_{29}S_{16}$
15	48.942(6)	1.8596(2)	1424(77)	0.196(12)	464(28)	Roxbyite(6,4,0),chalcocite, high, copper(I) sulfide(1,0,3)	$Cu_{29}S_{16}$, Cu_2S
16	54.71(3)	1.6763(8)	340(38)	0.24(3)	391(50)	Chalcocite, high, copper(I) sulfide(1,1,2)	Cu_2S
17	56.437(9)	1.6291(2)	190(28)	0.17(2)	570(83)	Chalcocite, high, copper(I) sulfide(2,0,1)	Cu_2S
18	61.32(3)	1.5107(6)	346(38)	0.37(5)	262(32)	Unknown	
19	73.45(2)	1.2882(3)	192(28)	0.13(4)	793(252)	Unknown	
20	74.92(9)	1.2665(13)	78(18)	0.34(17)	312(157)	Chalcocite, high, copper(I) sulfide(2,1,0)	Cu_2S

Name: **Roxbyite**	Name: **chalcocite**, high, copper(I) sulfide
Chemical Formula: $Cu_{29}S_{16}$	Chemical Formula: Cu_2S
Z value: 4	Z value: 2
Space Group: P-1(2)	Space Group: P63/mmc(194)
Cell: 13.4090 13.4051 15.4852 90.022 90.021 90.020	Cell: 3.9590 3.9590 6.7840 90.000 90.000 120.000
Volume: 2783.448	Volume: 92.085
Crystal System: Triclinic	Crystal System: Hexagonal
Reference: Mumme, W.G., Gable, R.W., Petricek, V. Can. Mineral. 50 (2012) 423.	Reference: Cava, R.J., Reidinger, F., Wuensch, B.J. Solid State Ionics 5 (1981) 501.

Table 2

Results of RFA $Cu_{1.80}S$

2-theta (deg)	d (ang.)	Height (cps)	FWHM (deg)	Size (ang.)	Phase name	Chemical formula
12.261(11)	7.213(7)	199(12)	0.115(17)	727(109)	Unknown	Unknown
20.929(5)	4.2411(10)	144(10)	0.06(9)	1445(2251)	Roxbyite(3,1,0)	$Cu_{29}S_{16}$
24.741(9)	3.5956(13)	141(10)	0.15(3)	563(123)	Roxbyite(2,3,-1), Copper Sulfide(1,1,0)	$Cu_{29}S_{16}$,CuS_2
26.55(3)	3.355(4)	374(16)	0.15(2)	559(79)	Roxbyite(2,-3,2), ?-Cu_2S(1,0,0)	$Cu_{29}S_{16}$,Cu_2S
27.79(3)	3.207(4)	80(7)	0.47(10)	182(40)	Roxbyite(2,-1,4)	$Cu_{29}S_{16}$
29.798(8)	2.9959(8)	274(14)	0.30(3)	289(25)	Roxbyite(2,-3,3),?-Cu_2S(1,0,1)	$Cu_{29}S_{16}$, Cu_2S
31.217(14)	2.8629(13)	482(18)	0.152(16)	566(60)	Roxbyite(1,3,-4)	$Cu_{29}S_{16}$
34.09(2)	2.6279(15)	568(20)	0.16(5)	552(187)	Roxbyite(5,1,0)	$Cu_{29}S_{16}$
35.435(7)	2.5312(5)	4395(54)	0.10(3)	859(220)	Roxbyite(0,4,-4), Copper Sulfide(1,1,1)	$Cu_{29}S_{16}$, CuS_2
36.366(4)	2.4685(3)	2765(43)	0.094(16)	932(160)	Unknown	Unknown
36.54(5)	2.457(3)	388(16)	0.26(4)	330(46)	Roxbyite(2,-5,-1), Copper Sulfide(1,2,0)	$Cu_{29}S_{16}$, CuS_2
37.882(13)	2.3731(8)	844(24)	0.22(4)	399(64)	Roxbyite(3,-2,5),?-Cu_2S(1,0,2)	$Cu_{29}S_{16}$, CuS_2
38.704(14)	2.3246(8)	471(18)	0.27(2)	320(24)	Unknown	Unknown
42.219(16)	2.1388(8)	267(13)	0.30(5)	300(49)	Copper Sulfide(2,1,0)	CuS_2
46.38(2)	1.9562(10)	275(14)	0.34(5)	267(43)	Roxbyite(6,2,3)	$Cu_{29}S_{16}$
46.910(5)	1.93527(18)	848(24)	0.26(2)	345(27)	Roxbyite(0,6,-4),?-Cu_2S(1,1,0)	$Cu_{29}S_{16}$, CuS_2
47.981(7)	1.8946(3)	155(10)	0.14(3)	627(116)	Roxbyite(5,-5,0)	$Cu_{29}S_{16}$
48.670(6)	1.8693(2)	604(20)	0.115(12)	794(86)	Unknown	Unknown
48.925(8)	1.8602(3)	1110(27)	0.213(13)	428(27)	Roxbyite(6,4,0),?-Cu_2S(1,0,3)	$Cu_{29}S_{16}$, Cu_2S
54.738(12)	1.6756(3)	274(14)	0.23(4)	403(63)	?-Cu_2S(1,1,2)	Cu_2S
56.496(17)	1.6275(4)	110(9)	0.26(5)	367(73)	?-Cu_2S(2,0,1)	Cu_2S
61.31(2)	1.5109(5)	394(16)	0.28(4)	349(49)	Copper Sulfide(0,2,2)	CuS_2
65.73(7)	1.4194(14)	95(8)	0.80(11)	123(17)	Copper Sulfide(3,0,1)	CuS_2
68.09(4)	1.3759(8)	119(9)	0.30(8)	335(91)	Unknown	Unknown
73.40(6)	1.2889(9)	137(10)	0.29(7)	360(86)	Copper Sulfide(1,4,1)	CuS_2
74.996(9)	1.26541(13)	956(25)	0.083(8)	1264(123)	Copper Sulfide(3,2,1)	CuS_2

Name: **Roxbyite**	Name: **Copper disulfide**
Chemical Formula: $Cu_{29}S_{16}$	Chemical Formula: CuS_2
Z value: 4	Z value: 2
Space Group: P-1(2)	Space Group: Pnnm(58)
Cell: 13.4090 13.4051 15.4852 90.022 90.021 90.020	Cell: 4.6510 5.7930 3.5320 90.000 90.000 90.000
Volume: 2783.448	Volume: 95.164
Crystal System: Triclinic	Crystal System: Orthorhombic
Reference: Mumme, W.G., Gable, R.W., Petricek, V. Can. Mineral. 50 (2012) 423.	Reference: Kjekshus, A., Rakke, T. Acta Chem. Scand., Ser. A33(1979)617.

Table 3

Results of RFA $Cu_{1.75}S$

2-theta (deg)	d (ang.)	Height (cps)	FWHM (deg)	Size (ang.)	Phase name	Chemical formula
20.931(11)	4.241(2)	117(9)	0.11(5)	772(368)	Roxbyite(3,-1,0)	$Cu_{58}S_{32}$
24.70(2)	3.601(3)	135(10)	0.15(4)	575(150)	Roxbyite(1,-1,-4),Djurleite, syn(7,1,1)	$Cu_{58}S_{32}$, $Cu_{31}S_{16}$
26.55(3)	3.355(3)	313(15)	0.18(3)	486(93)	Roxbyite(2,-3,2),Djurleite, syn(8,0,0)	$Cu_{58}S_{32}$, $Cu_{31}S_{16}$
29.802(8)	2.9955(8)	272(14)	0.34(3)	253(20)	Roxbyite(2,-2,-4),Djurleite, syn(4,0,-4)	$Cu_{58}S_{32}$, $Cu_{31}S_{16}$
31.181(7)	2.8661(6)	621(20)	0.104(13)	829(107)	Roxbyite(1,-3,-4),Djurleite, syn(9,1,-1)	$Cu_{58}S_{32}$, $Cu_{31}S_{16}$
34.09(2)	2.6278(19)	461(18)	0.18(2)	474(55)	Roxbyite(5,-1,0),Djurleite, syn(4,5,-2)	$Cu_{58}S_{32}$, $Cu_{31}S_{16}$
35.39(2)	2.5342(17)	415(17)	0.20(5)	432(116)	Roxbyite(5,0,2),Djurleite, syn(2,6,-1)	$Cu_{58}S_{32}$, $Cu_{31}S_{16}$
36.399(6)	2.4663(4)	2192(38)	0.160(7)	545(24)	Djurleite, syn(3,5,3)	$Cu_{31}S_{16}$
37.571(11)	2.3920(7)	374(16)	0.58(5)	152(14)	Djurleite, syn(11,1,0)	$Cu_{31}S_{16}$
37.928(3)	2.37030(17)	653(21)	0.135(18)	648(88)	Roxbyite(1,-2,-6)	$Cu_{58}S_{32}$
42.24(4)	2.1380(19)	380(16)	0.34(5)	263(37)	Roxbyite(2,-3,-6),Djurleite, syn(9,2,4)	$Cu_{58}S_{32}$, $Cu_{31}S_{16}$
43.296(3)	2.08809(13)	550(19)	0.064(11)	1399(248)	Copper, syn(1,1,1)	Cu
46.403(10)	1.9552(4)	515(19)	0.26(2)	343(27)	Djurleite, syn(3,7,-3)	$Cu_{31}S_{16}$
46.90(2)	1.9356(8)	795(23)	0.26(2)	344(28)	Roxbyite(0,0,8),Djurleite, syn(5,6,-4)	$Cu_{58}S_{32}$, $Cu_{31}S_{16}$
48.630(11)	1.8708(4)	704(22)	0.129(15)	705(80)	Djurleite, syn(2,8,-2)	$Cu_{31}S_{16}$
48.925(15)	1.8602(5)	1015(26)	0.24(3)	383(42)	Roxbyite(4,-3,-6)	$Cu_{58}S_{32}$
54.75(4)	1.6753(13)	256(13)	0.32(7)	292(65)	Roxbyite(8,0,0)	$Cu_{58}S_{32}$
56.46(7)	1.6284(18)	141(10)	0.24(8)	400(129)	Roxbyite(2,-4,-8)	$Cu_{58}S_{32}$
61.30(4)	1.5110(9)	280(14)	0.36(7)	265(48)	Unknown	Unknown
73.39(12)	1.2891(17)	111(9)	0.72(15)	144(31)	Copper, syn(2,2,0)	Cu

Name: **Roxbyite**	Name: **Djurleite**, syn
Chemical Formula: $Cu_{29}S_{16}$	Chemical Formula: $Cu_{31}S_{16}$
Z value: 4	Z value: 8
Space Group: P-1(2)	Space Group: P21/n(14)
Cell: 13.4090 13.4051 15.4852 90.022 90.021 90.020	Cell: 26.8970 15.7450 13.4650 90.000 90.130 90.000
Volume: 2783.448	Volume: 5702.322
Crystal System: Triclinic	Crystal System: Monoclinic
Reference: Mumme, W.G., Gable, R.W., Petricek, V. Can. Mineral. 50 (2012) 423.	Reference: Potter, II, R., Evans, Jr. J. Research U. S. Geol. Surv.4 (1976) 205.

X-ray phase analysis was performed on a Bruker diffractometer (Germany) using radiation from a CuKa X-ray tube and a graphite monochromator on a diffracted beam. Diffractograms were recorded in the range of angles 2θ from 20 to 110, with a step of 2θ = 0.02. The BrukerAXSDIFFRAC.EVAv software was used to identify the phases.4.2 and the international database ICDD PDF-2.

$Cu_{1.75}S$ samples at room temperature contain the rhombic phase of anilite with parameters a = 7.8902 and 7.8938 Å, b = 7.8408 and 7.8433 Å, c = 11.011 and 11.012 Å, respectively, and the hexagonal phase of digenite with the spatial group R-3m (166) and parameters a = 3.94310 Å and 3.94437 Å, c = 48.43262 Å and 48.43325 Å respectively.

The difference in the parameters of the crystal lattice due to changes in the interplane distances of samples with different sodium content, as well as the broadening of diffraction lines on diffractograms, may be due to microstresses in the structure, which are associated with the accumulation of dislocations, as well as the fragmentation of crystallites associated with crystallization processes. The analysis of the angular de-

pendence of the physical broadening makes it possible to assess the influence of both factors. The Williamson-Hall method was used to assess the impact.

The size of the crystallites was estimated based on the width of the X-ray lines. The crystallite sizes in all samples range from 30 to 90 nm, which is due to the method of synthesis of sodium and potassium hydroxides in the melt.

Phase transitions and thermal effects in the Cu_2S sample were studied using the DSC 404 F1 Pegasus device (NETZSCH, Germany) in an argon atmosphere in the temperature range (300–600) K. The heating rate was 10 K/min.

To calculate the heat capacity, three different measurements were carried out: baseline, standard (sapphire) and the test sample. The following parameters remained identical in all measurements: argon flow, argon flow rate, initial temperature, heating rate, mass of the crucible and lid, the crucibles on the sensor were oriented, maintaining their position on the sensor. During the measurement, a program was used that includes holding the sample at a constant temperature (at least half an hour) in an argon current, after which heating was carried out at a constant rate of 5 K/min. Measurements of the baseline and standard were carried out in the same mode. The DSC 404 F1 Pegasus allows for a calorimetric experiment with a small sample quantity, we used sample weights from 40 to 150 mg.

Figure 1 shows the curves of the Cu_2S DSC. There is an acute endothermic peak of DSC, the temperature of which lies within 381.5 K, depending on the composition. Heat capacity peaks are observed at the same temperatures.

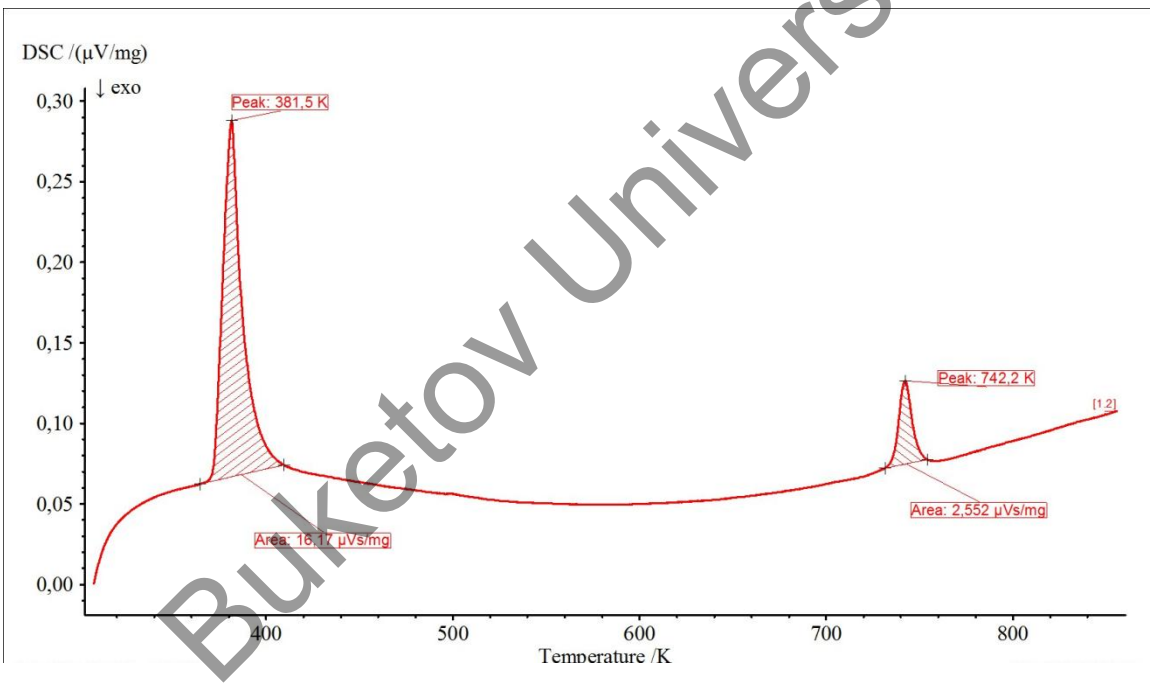

Figure 1. DSC curves of the sampleCu_2S

The structure of Cu_2S copper sulfide ((chalcosine), close to stoichiometric, according to Abrikosov N.H. [4]) has three modifications: orthorhombic below 105 °C, hexagonal below (420–450) °C and high-temperature cubic (phase). Figure 2 shows an image taken with a scanning electron microscope from the surface of Cu_2S powder obtained by electrohydrodynamic impact. It can be seen that the particles have the shape of ribbons and wires ranging in size from fractions of a micron to tens of microns.

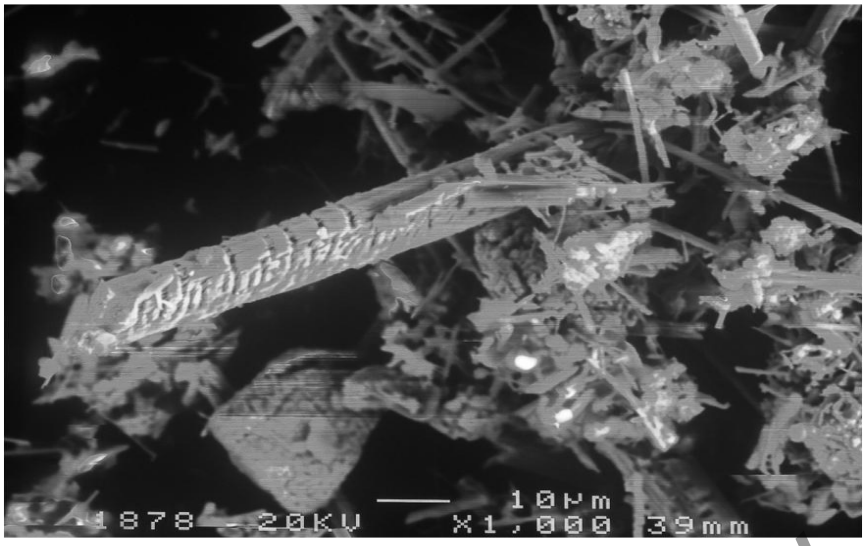

Figure 2. A snapshot of Cu_2S powder on a scanning electron microscope

Thermal conductivity measurements were carried out using the flash method on the LFA 467 HT HyperFlash device (NETZSCH, Germany). Thermal conductivity (k) was found from three measurements:

$$k(T) = a(T) * \rho(T) * c_p(T),$$

where T is temperature, k is thermal conductivity, a is thermal conductivity, ρ is bulk density, c_p is specific heat capacity.

The thermal conductivity a was determined using the LFA 467 HT installation according to the Parker formula from the analysis of the time dependence of the temperature of the opposite side of the sample after short-term heating of one side of the sample by a powerful light pulse. The values of the c_p heat capacity were measured on a DSC 404 F1 Pegasus DSC calorimeter (NETZSCH, Germany) in an argon atmosphere. The density of the sample was found from measurements of weight and volume. Figure 2 shows the temperature dependences of the thermal conductivity, heat capacity and thermal conductivity of Cu_2S.

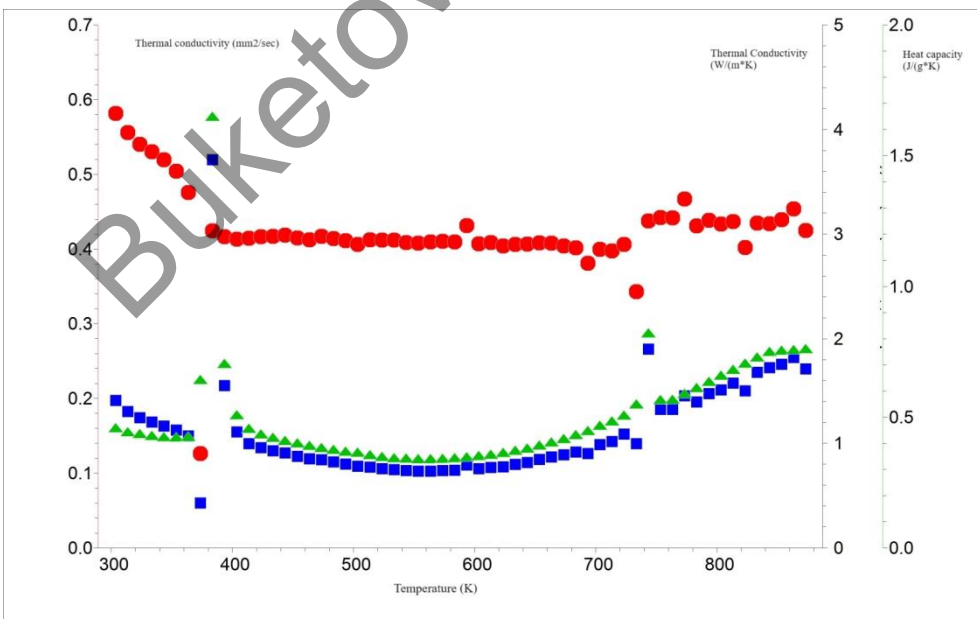

Figure 3. Temperature dependence of thermal conductivity Cu_2S

The thermal conductivity of the Cu_2S sample is quite low, it rises to 0.3 W/m*K at a phase transition of about 380 K and does not fall below 0.2 W/m*K.

In the semiconductor under consideration, the concentration of impurity carriers of electrons in the conduction band and holes in the valence band is usually much higher than the concentration of uncontrolled impurities and equilibrium point defects. The concentration of n_i native carriers is determined by the temperature and the width of the band gap. In most cases, n_i is also significantly less than n_t. In this case, the temperature dependence of the electronic conductivity is determined by the temperature dependence of the mobility and has a metallic character [5, 6]. Figure 4 shows the temperature dependence of the electron thermo-emf coefficient of the Cu_2S sample.

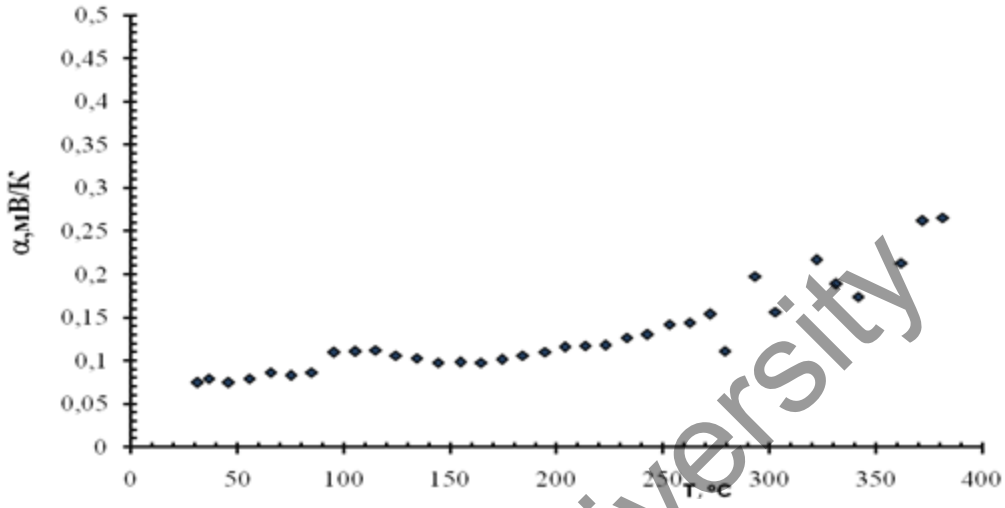

Figure 4. Temperature dependence of the coefficient of electronic thermo-emf of a coarse-grained sample Cu_2S

The coefficient of thermal EMF strongly depends on the nonstoichiometry of the sample and is maximum for a composition close to saturation with copper. The temperature dependence of the electron thermal emf coefficient of the Cu_2S sample has rather low values here from 0.05 mV/K to 0.25 mV/K, which are more typical for metals than for semiconductors.

Figure 5 shows the temperature dependence of the electron conductivity of coarse-grained Cu_2S. It can be seen from the figure that the semiconductor temperature dependence of about 185 °C changes to a metallic type of dependence.

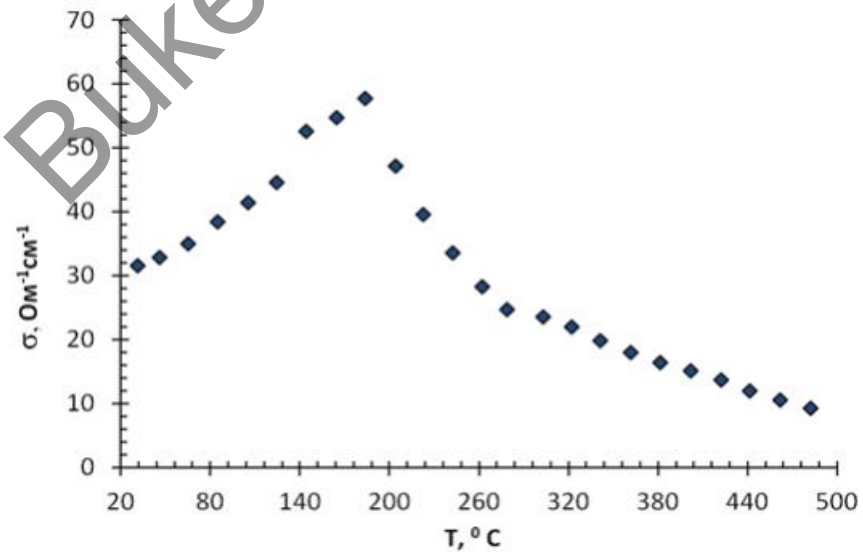

Figure 5. Temperature dependence of the conductivity of a large-crystal Cu_2S

During annealing, the conductivity of polycrystalline samples usually increases with grain growth, and a similar dependence is observed here. The reasons for this behavior of kinetic coefficients are changes in the

specific gravity in the total volume of grain boundary layers, which increase the concentration of defects — scattering centers for current carriers.

For the Cu_2S sample, a phase transition of about 400 K is clearly visible on the temperature dependence of the conductivity (according to the literature data — 403 K), corresponding peaks are also present on the temperature dependence of the DSC.

Conclusion

Copper chalcogenides have a complex electronic structure due to the interaction of hybridized *s*- and *p*-states of chalcogen forming a valence band with 3*d* states of copper [7, 8], which greatly complicates the interpretation of temperature dependences of kinetic parameters having a nonmonotonic character.

Cu_2S copper sulfide is an effective thermoelectric material, so it is interesting to study its kinetic parameters of solid solutions that it forms with alkali metals. The nonstoichiometry of chalcogenides can be easily controlled electrochemically, therefore, the task of selecting the optimal composition according to the cationic sublattice is quite feasible. In addition, to improve the thermoelectric properties, it can be achieved by alloying lithium into a binary copper sulfide matrix, we obtained a high ZT with local maxima that reaches up to 2 [9]. When doped with sodium, this indicator reached up to 1 [10, 11]. Thus, the work on the synthesis of copper sulfides of different composition and morphology is in the current trend of searching for new thermoelectric materials and allows us to hope for practical application of the obtained materials in the near future.

Acknowledgments

The Science Committee of the Republic of Kazakhstan, which is part of the Ministry of Science and Higher Education, provided funding for this research (No. AP14871197).

References

1 Chopra, K. & Das, S. (1986). Thin−film solar cells. Moscow: Mir, 435 p.

2 Scheer, R. & Schock, H.-W. (2011). *Chalcogenide Photovoltaics: Physics, Technologies, and Thin Film Devices*. Ed. 2011 WILEY-VCH Verlag & Co. KGaA, Germany, 386.

3 Okimura, H., Matsumae, T., & Makabe, R.J.T.S.F. (1980). Electrical properties of $Cu_{2-x}Se$ thin films and their application for solar cells. *Thin Solid Films, 71*(1), 53–59.

4 Abrikosov, N.H., Bankina, V.F., Poretskaya, L.V., Skudnova, E.V., & Chizhevskaya, S.N. (1975). Semiconductor chalcogenides and alloys based on them. Moscow: Nauka, 220 p.

5 Berezin, V.M. & Vyatkin, G.P. (2001). Superionic semiconductor chalcogenides. Chelyabinsk: Publishing house of South Ural State University, 135 p.

6 Khassenov, A.K., Karabekova, D.Zh., Nussupbekov, B.R., G.A. Bulkairova, A.S. Kudusov, Alpysova, G.K., & Bolatbekova, M.M. (2023). Investigation of the influences of pulsed electrical discharges on the grinding of quartz raw materials. *Bulletin of the University of Karaganda – Physics, 2*(110), 93–99.

7 Domashevskaya, E.P., Terekhov, V.A., Kashkarov, V.M., Panfilova, E.P., Gorbachev, V.V., & Shchukarev, A.V. (2000). *d-p* resonance in some copper chalcogenides according to X-ray ultra-soft emission and X-ray photoelectron spectroscopy data. *Condensed media and interphase boundaries, 2*(4), 353–357.

8 Lavrentiev, A.A., Nikiforov, I.Ya., Dubeyko, V.A., Gabrelyan, B.V., Domashevskaya, E.P., Rehr, J.J., & Ankudinov, A.L. (2001). *d-p*-resonance effect in copper compounds with various crystalline structures. *Condensed media and interphase boundaries, 3*(4), 107–121.

9 Balapanov, M.H., Kuterbekov, K.A., Ishembetov, R.H., Kurbanova, M.M., Kabyshev, A.M., Bekmyrza, K., & Yakshibaev, R.A. New thermoelectric material $Li_{0.15}Cu_{1.85}S$ Eurasian patent No.030605, 08/31/2018.

10 Balapanov, M.Kh., Ishembetov, R.Kh., Kuterbekov, K.A., Almukhametov, R.F., & Yakshibaev, R.A. (2018). Transport phenomena in superionic $Na_xCu_{2-x}S$ (x = 0,05; 0,1; 0,15; 0,2) compounds. *Ionics, 24*(5), 1349–1356. DOI:10.1007/s11581-017-2299-z

11 Kuterbekov, K.A., Balapanov, M.K., Kubenova, M.M., Ishembetov, R.Kh., Zeleev, M.Kh., Yakshibaev, R.A., Kabyshev, A.M., Alina, R.A., Bekmyrza, K.Zh., Baikhozhaeva, B.U., Abseitov, E.T., & Taimuratova, L.U. (2022). Chemical diffusion and ionic conductivity in nonstoichiometric nanocrystalline superionic $Na_xCu_{1.75}S$ (x = 0.1, 0.15, 0.2, 0.25) materials. *Ionics, 28*, 4311–4319. https://doi.org/10.1007/s11581-022-04651-y

М.М. Кубенова, К.А. Кутербеков, М.Х. Балапанов, Р.Х. Ишембетов,
Г.Д. Кабдрахимова, Р.А. Алина, М. Татай, Р. Ильдос

Cu_2S бинарлы мыс сульфидінің жылулық қасиеттері

Мыс халькогенидтері валенттік аймақты құрайтын гибридтелген *s*- және *p*- халькоген күйлерінің 3*d* мыс күйлерімен өзара әрекеттесуіне байланысты күрделі электрондық құрылымға ие, бұл қасиеттер монотонды емес сипаттағы кинетикалық параметрлердің температураға тәуелділігін интерпретациялауды қиындатады. Cu_2S мыс сульфиді тиімді термоэлектрлік материал болып табылады, сондықтан оның сілтілі металдарды құрайтын қатты ерітінділерінің кинетикалық параметрлерін зерттеу өте қызықты. Мақалада Cu_2S бинарлы мыс сульфидінің қасиеттерінің эксперименттік зерттеулер нәтижелері ұсынылған. Cu_2S үлгісі үшін жартылай өткізгіштерге қарағанда металдарға тән 0,05 мВ/К-ден 0,25 мВ/К-ге дейінгі үлгінің электронды термо-эқк өте төмен мәндері анықталды. Cu_2S үлгісінің жылу өткізгіштігі өте төмен, ол шамамен 380 К фазалық ауысу кезінде 0,3 Вт/м*К-ге дейін көтеріледі және 0,2 Вт/м*К-ден төмен түспейді. Сонымен қатар халькогенидтерді стехиометриясыз электрхимиялық оңай басқаруға болады, сондықтан катиондық қосалқы тор негізінде оңтайлы құрамды таңдау әбден мүмкін. Сондай-ақ Cu_2S термоэлектрлік қасиеттерін жақсарту үшін мыс сульфидінің бинарлы матрицасына сілтілі металдарды легирлеу кезінде қол жеткізуге болады.

Кілт сөздер: термоэлектрлік материалдар, мыс сульфиді, кристалдық құрылым, өткізгіштік, жылу өткізгіштік, Зеебек коэффициенті, суперионды өткізгіштер.

М.М. Кубенова, К.А. Кутербеков, М.Х. Балапанов, Р.Х. Ишембетов,
Г.Д. Кабдрахимова, Р.А. Алина, М. Татай, Р. Ильдос

Тепловые свойства бинарного сульфида меди Cu_2S

Халькогениды меди обладают сложной электронной структурой из-за взаимодействия гибридизованных *s*- и *p*- состояний халькогена, образующих валентную зону, с 3*d*-состояниями меди, что сильно затрудняет интерпретацию температурных зависимостей кинетических параметров, имеющих немонотонный характер. Сульфид меди Cu_2S является эффективным термоэлектрическим материалом, поэтому интересно исследовать его кинетические параметры твердых растворов, которые он образует с щелочными металлами. Нестехиометрией халькогенидов можно легко управлять электрохимически, поэтому задача подбора оптимального состава по катионной подрешетке является вполне осуществимой. В статье представлены экспериментальные исследования свойств бинарного сульфида меди Cu_2S. Для образца Cu_2S обнаружены довольно низкие значения коэффициента электронной термо-эдс образца от 0,05 мВ/К до 0,25 мВ/К, характерные более для металлов, чем для полупроводников. Теплопроводность образца Cu_2S является достаточно низкой, она поднимается до 0,3 Вт/м*К при фазовом переходе около 380 К и не опускается ниже 0,2 Вт/м*К. Таким образом, нестехиометрией халькогенидов можно легко управлять электрохимически, поэтому задача подбора оптимального состава по катионной подрешетке является вполне осуществимой. Кроме того, улучшения термоэлектрических свойств Cu_2S можно достичь при легировании щелочных металлов в матрицу бинарного сульфида меди.

Ключевые слова: термоэлектрические материалы, сульфид меди, кристаллическая структура, проводимость, теплопроводность, коэффициент Зеебека, суперионные проводники.

Information about authors

Kubenova, M.M. — PhD, Research teacher, Department of Standardization and Certification, L.N. Gumilyov Eurasian National University, Astana, Kazakhstan. ORCID: https://orcid.org/0000-0003-2012-2702

Kuterbekov, K.A. — Doctor of physical and mathematical sciences, Professor of the International Department of Nuclear Physics, new materials and technologies, L.N. Gumilyov Eurasian National University, Astana, Kazakhstan. ORCID: https://orcid.org/0000-0001-7116-1520

Balapanov, M.Kh. — Doctor of physical and mathematical sciences, Professor of the Department of General Physics, Ufa University of Science and Technology, Ufa, Russia. ORCID: https://orcid.org/0000-0001-788 5-9462

Ishembetov, R.Kh. — Candidate of physical and mathematical sciences, Docent of the Department of General Physics, Ufa University of Science and Technology, Ufa, Russia. ORCID: https://orcid.org/0000-0002-0938-3998

Kabdrakhimova, G.D. — PhD, Associate professor of the International Department of Nuclear Physics, new materials and technologies, L.N. Gumilyov Eurasian National University, Astana, Kazakhstan. ORCID: https://orcid.org/0000-0003-2453-1028

Alina, R.A. — Doctoral student, L.N. Gumilyov Eurasian National University, Astana, Kazakhstan.

Tatay, M. — Student, L.N. Gumilyov Eurasian National University, Astana, Kazakhstan.

Ildos, R. — Student, L.N. Gumilyov Eurasian National University, Astana, Kazakhstan.

Article

Received: 25.09.2023
Accepted: 08.12.2023

UDC 533.9.07

https://doi.org/10.31489/2024PH1/23-33

L.G. Sulyubayeva[1, 2], B.K. Rakhadilov[1], Y. Naimankumaruly[1], M.B. Bayandinova[1], N. Muktanova[1], N.E. Berdimuratov[2*]

[1]*PlasmaScience LLP, Ust-Kamenogorsk, 070000, Kazakhstan;*
[2]*Research Center Surface Engineering and Tribology, Sarsen Amanzholov East Kazakhstan University, Ust-Kamenogorsk, 070000, Kazakhstan*
[*]*Corresponding author's e-mail: nurbol.ber@gmail.com)*

Study of changes in the surface structure of tungsten irradiated by helium plasma

One of the important aspects is the interaction of plasma with the surface of a material, especially in the conditions of a fusion facility. The current work presents the preliminary results of the study of tungsten surface structure modification under helium plasma irradiation. A small-sized linear simulator KAZ-PSI with a plasma-beam setup was designed and assembled, where helium was used as a working gas. The main elements of the linear plasma simulator are an electron beam gun with a LaB6 cathode, a plasma-beam discharge chamber, an interaction chamber, a target device, and an electromagnetic system consisting of electromagnetic coils. It was revealed that under irradiation on the surface of the samples there is a relief with defective structure consisting of chaotically arranged ledges and pits of various shapes with average size (100–600) nm and pore sizes (0.1–1.5) μm with visible areas of flaking and sputtering. It was found that when the negative potential on the target is varied by –500V/–1000V/–1500V, the formation of dislocation with chaotic and cellular structure of tungsten with an average grain size of (1–25) μm is observed; it was revealed that the total values of elastic and plastic components of deformation across the tungsten grain differ from each other by about 2.5 times.

Keywords: tungsten, helium plasma, structure, surface modification, quantitative parameters of fine structure, plasma generator, surface.

Introduction

As it is known, to the present day, the successful implementation of the International Thermonuclear Experimental Reactor (ITER) project and new advances in next-generation nuclear fusion reactors such as ITER and China Fusion Engineering Test Reactor (CFETR), Demonstration Fusion Power Plant (DEMO) contribute to the development of nuclear energy and fusion and bring them to a new frontier [1–3]. Materials in fusion devices withstand severe exposure to high-temperature plasma, which promotes the development of radiation defects and subsequently leads to material damage. Therefore, the problem of improving the properties and performance characteristics of materials remains one of the important tasks for fusion energy [4]. According to the authors of the review paper [5] in the ITER facility [1], protective materials must withstand three conditions simultaneously: first, the effects of surface sputtering, blistering, and erosion during the interaction of the particles flying out of the plasma without excessive contamination of the core plasma; second, due to the rapid release of energy during plasma rupture, a relatively high steady-state surface heat load of ~10 $MW \cdot m^{-2}$ and a transient heat load of ~20 $MW \cdot m^{-2}$ are released; third, resistance to damage from neutron radiation with energy 14.1 MeV, embrittlement from hydrogen (H) isotope (deuterium (D) and tritium (T))/helium (He) and gas swelling.

Along with other energy sources, nuclear fusion is seen as the most promising alternative to fossil fuels for a future carbon-free energy system. ITER, currently the largest fusion device under construction, is expected to provide a high thermal output of ~150 MW [6]. However, the extreme conditions created during ITER operation pose significant challenges for the plasma facing materials (PFM) in the divertor of the fusion device; e.g., high heat flux deposition and particle bombardment. In the background of nuclear fusion reactor devices such as ITER and DEMO, tungsten (W) is considered as a potential and one of the most promising candidate PFM materials for plasma facing components (PFC) due to its high melting point, good thermal conductivity, low sputtering yield and low hydrogen solubility [7–8].

Helium atoms, which have low solubility in metals, can lead to undesirable changes in material properties, such as the formation of nanopores and bubbles [9, 12–13], blisters, etc. Experiments to determine the influence of helium performed in reactor experiments are very challenging due to the requirement for pro-